J. Fluid Mech. (2013), *vol.* 729, *pp.* 496–523. © Cambridge University Press 2013
doi:10.1017/jfm.2013.324

The Faraday threshold in small cylinders and the sidewall non-ideality

W. Batson[1,2,†], F. Zoueshtiagh[2] and R. Narayanan[1]

[1]Department of Chemical Engineering, University of Florida, Gainesville, FL 32601, USA

[2]Université Lille 1, Institut d'Electronique, de Microélectronique et de Nanotechnologie (IEMN), UMR, CNRS 8520, Avenue Poincaré, 59652 Villeneuve d'Ascq, France

(Received 25 October 2012; revised 13 June 2013; accepted 19 June 2013;
first published online 24 July 2013)

In this work we investigate, by way of experiments and theory, the Faraday instability threshold in cylinders at low frequencies. This implies large wavelengths where effects from mode discretization cannot be ignored. Careful selection of the working fluids has resulted in an immiscible interface whose apparent contact line with the sidewall can glide over a tiny film of the more wetting fluid, without detachment of its actual contact line. This unique behaviour has allowed for a system whose primary dissipation is defined by the bulk viscous effects, and in doing so, for the first time, close connection is seen with the viscous linear stability theory for which a stress-free condition is assumed at the sidewalls. As predicted, mode selection and co-dimension 2 points are observed in the experiment for a frequency range including subharmonic, harmonic, and superharmonic modes. While agreement with the predictions are generally excellent, there are deviations from the theory for certain modes and these are explained in the context of harmonic meniscus waves. A review of previous work on single-mode excitation in cylinders is given, along with comparison to the viscous model and analysis based upon the conclusions of the current experiments.

Key words: Faraday waves, instability

1. Introduction

Faraday instability is a result of the parametric resonance of interfacial wave modes with an imposed vibrational frequency. The forcing amplitude at which the mode appears is proportional to its dissipation and the excited wavelength is generally specified by the wave whose natural frequency is half that of the parametric excitation frequency. Experimentally, this generalization is valid at a large frequency where the excited wavelength is much smaller than the cell container and the system has access to a continuum of modes. Experimental connection has been made in past work between the onset amplitudes with the predictions of the viscous linear stability theory in the high-frequency regime, but remains elusive in the low-frequency regime of single-mode excitation. Aside from a scientific interest in delineating mode interaction, low-frequency mode excitation is also of practical interest such as in Faraday-induced

† Email address for correspondence: wbatson@gmail.com

https://doi.org/10.1017/jfm.2013.324 Published online by Cambridge University Press

fluid mixing in narrow geometries (Zoueshtiagh, Amiroudine & Narayanan 2009; Friend & Yeo 2011).

At low frequency, where the preferred wavelength is large, mode discretization becomes a factor and the excitation of a mode whose natural frequency is twice that of the forcing is no longer guaranteed. In this regime the same mode of instability can be excited for an entire band of frequencies, whose associated threshold amplitudes descend to a minimum amplitude near the natural frequency of that mode. The modes excited at frequencies above and below the natural frequency are referred to as tuned and detuned modes. Previous measurements of threshold amplitudes of these bands of modes have used fluid systems in which viscous damping in the interior of the wave is negligible compared to the damping effects of the sidewalls and are extremely challenging to model. Often, however, the sidewall damping in these systems has been taken to be linear, and the onset thresholds have therefore been described using single degree of freedom system theory (Nayfeh & Mook 1979). To our knowledge, no previous attempts have been made to produce an ideal experimental system in which modes are discretized but whose damping is controlled by the interior, thereby allowing connection to the viscous linear theory of Kumar & Tuckerman (1994). This, therefore, is the primary goal of this work.

The complexity of the sidewall behaviour is a difficulty in both high and low-frequency Faraday experiments. The mathematically tractable boundary condition at the container sidewalls is the so-called stress-free condition, which places constraints on the allowed dynamics of the interface near the sidewall. A physically realistic interface and its contact with the sidewall suffers from complex dynamics and additional dissipation due to meniscus formation, contact line mobility, and stresses from sidewall fluid shearing. Due to the periodic modulation of its desired shape, the meniscus emits a travelling wave from the sidewall to the interior for each period of cell motion. High-frequency experiments have employed different filling techniques to eliminate meniscus waves and the issues of contact line mobility have been circumvented by using viscous fluids which damp out the non-ideality and allow the interior to behave as a laterally infinite system. Bechhoefer *et al.* (1995) successfully produced such a system with paraffin oils with temperature-controlled viscosity ranging from 25 to 200 cSt and a brimful condition. Their experiments were motivated by earlier experiments, such as those of Fauve *et al.* (1992), which highlighted a need for a better understanding of the workings of viscosity, as high-frequency matching of the thresholds was not obtained by incorporation of linear damping in the inviscid model. The experiments of Christiansen, Alstrøm & Levinsen (1994) are of note as they consider the model of Milner (1991) for contact line behaviour and obtain good matching at remarkably high frequencies ranging from 100 to 500 Hz. Experiments with two immiscible liquids were performed by Kityk *et al.* (2005), who attempted to verify the viscous theory.

The upper range of the experiments of Bechhoefer *et al.* (1995) was roughly 80 Hz, but what motivates the current work is the lower limit they explored with frequencies as low as 6 Hz. The instability threshold matched well with the theory at high frequencies, but at low frequencies there appeared ‘oscillations’ in the threshold, which they attributed to the discretization of the modes available to the system. Douady (1990) performed experiments in the regime where modes are discretized, for both a system with a prominent meniscus and a system with a pinned contact line using a brimful condition. With the meniscus, the critical thresholds did not show sharp discretization, and without the meniscus these experiments showed discretization similar to that of Bechhoefer *et al.* (1995). The experiments of both Bechhoefer *et al.*

https://doi.org/10.1017/jfm.2013.324 Published online by Cambridge University Press

and Douady highlight the important effects of mode discretization, but it must be noted that the observed thresholds for modes with a brimful condition cannot be predicted by the viscous theory incorporating a stress-free boundary condition as the sets of allowed eigenfunctions are different for the two cases.

While meniscus waves are deemed detrimental to the high-frequency threshold, they have been ignored in single-mode experiments and contact line mobility has been prioritized. The contact line motion at the sidewalls is of extreme importance as it has been shown to introduce considerable amounts of dissipation to the system. A model describing this dissipation is enormously complex, requiring a connection to be made between the molecular, boundary layer, and container scales. The importance of these scales has been revealed by experiments such as that of Keulegan (1958), who established that sidewall surface wetting played a key factor in the decay of water waves, as identical experiments produced far greater damping rates in Lucite containers than in glass containers. The addition of aerosol lowered the surface tension, bringing the damping rates in the two containers into agreement. Miles (1967) developed a model for the damping of waves for slightly viscous fluids that separately treated the contributions due to wall boundary layers, surface films produced by contamination, and capillary hysteresis. Application of this model to the wave damping results of Case & Parkinson (1957) and Keulegan (1958) yielded qualitative explanations for their observed damping rates but not quantitative. In applying the model to the single-mode Faraday experiments of Henderson & Miles (1990), it was seen that the rates were correctly predicted provided that the water viscosity was taken to be 3 cSt. Upon using this damping rate the stability model used by Henderson & Miles (1990) was able to accurately predict the Faraday instability threshold for the fundamental axisymmetric mode in their cylindrical cell. While it is remarkable that this match was produced, what will be shown is that the threshold behaviour is characteristically different from the predictions for a system whose dissipation is controlled by the interior of the wave.

The focus of this work is therefore to produce an experiment that respects the sidewall stress-free boundary condition, thereby permitting both a closer approximation to the theory of Kumar & Tuckerman (1994) and isolation of the causes for the differences. This was accomplished by using two immiscible liquids, i.e. FC70 and silicone oil, producing an interface that could undergo apparent free motion at the sidewalls on top of a film produced by the silicone oil. This system of fluids has allowed us to very nearly realize both the frequencies and amplitudes at which modes are predicted to appear by the viscous linear stability theory using a stress-free boundary condition. Measurement of the damping rates confirms that the experiment is controlled by the interior damping. Explanations for the deviation between the observed and predicted threshold can be posited as being attributed to the meniscus and the number of azimuthal nodes. First we present the linear stability theory of Kumar & Tuckerman (1994) in a practical manner, along with the adaptation to a cylindrical cell with mode discretization. We then analyse the previous reports of the Faraday threshold in small cylinders in the context of this model. We finally present the experimental results of this work and their dominant features.

2. The model

2.1. *Spatially infinite systems*

To analyse the stability of a flat immiscible interface subjected to an oscillatory vertical motion of $A\cos\omega t$ with stress-free sidewalls we first follow the method of

https://doi.org/10.1017/jfm.2013.324 Published online by Cambridge University Press

Kumar & Tuckerman (1994), who consider a horizontally infinite fluid bilayer of mean depths h_1 and h_2 separated by an interface whose interfacial tension is denoted by γ. We then observe that the case of stress-free sidewalls can be adapted from the horizontally infinite fluid analysis. The equations of motion for the flow in the bulk domains are written in a reference frame that moves with the imposed motion, resulting in the grouping of the forcing acceleration $A\omega^2 \cos \omega t$ with the gravitational acceleration, g. Thus we have

$$\rho_j \left(\frac{\partial \boldsymbol{V}_j}{\partial t} + \boldsymbol{V}_j \cdot \boldsymbol{\nabla} \boldsymbol{V}_j \right) = -\boldsymbol{\nabla} P_j + \mu_j \nabla^2 \boldsymbol{V}_j + \rho_j (g + A\omega^2 \cos \omega t) \boldsymbol{e}_z \tag{2.1}$$

$$\boldsymbol{\nabla} \cdot \boldsymbol{V}_j = 0, \tag{2.2}$$

where $j = 1$ indicates the lower layer and $j = 2$ the upper. The vector $\boldsymbol{V}$ is the velocity of the fluids of pressure P, of density ρ and of viscosity μ. No-slip conditions apply at the top and bottom walls, and continuity of velocity is applied at the interface. The interface is a material surface, thus the kinematic condition leads to

$$(\boldsymbol{V} - \boldsymbol{U}) \cdot \boldsymbol{n} = 0 \quad \text{at } z = Z(x, y, t), \tag{2.3}$$

where $\boldsymbol{U} \cdot \boldsymbol{n}$ is the speed of the interface, $\boldsymbol{n}$ being the surface normal pointing into the light fluid, and $z = Z(x, y, t)$ is the position of the deflecting interface. The continuity of velocity components holds at the interface. The stress balance at the interface,

$$[\![-P\boldsymbol{I} + \mu(\boldsymbol{\nabla} \boldsymbol{V} + (\boldsymbol{\nabla} \boldsymbol{V})^{\mathrm{T}})]\!] \cdot \boldsymbol{n} = \gamma 2H \boldsymbol{n} \quad \text{at } z = Z(x, y, t), \tag{2.4}$$

states that the pressure and viscous tangential stress differences between the two phases are balanced by the forces arising from surface curvature, where γ is the interfacial tension and $2H$ is twice the mean surface curvature. Here the braces represent a jump quantity, evaluated as $[\![Q]\!] = Q_2 - Q_1$.

The system velocities, pressures, and the free surface variables are expanded in powers of a small parameter, ϵ. The solution to the zeroth-order problem is the base state, where the velocities are zero and the interfacial deflection is also zero. What is learnt is that the vertical base pressure gradient is balanced by the oscillating acceleration. The linear stability of the entire system can then be cast into the normal component of the stress balance at first order, written at the reference surface, $z = 0$, as

$$[\![p - 2\mu \partial_z w]\!] - (\rho_2 - \rho_1)(g + A\omega^2 \cos \omega t)\zeta + \gamma(\partial_{xx} + \partial_{yy})\zeta = 0 \tag{2.5}$$

where p is the perturbed pressure, w is the perturbed vertical component of velocity, and ζ is the perturbed free surface. In the above, the subscripts x, y and z on ∂ represent the partial derivative operator. It may be noted that the linearized domain equations and the kinematic conditions relate p and w to ζ, thereby yielding a homogeneous problem in ζ.

The perturbed system is analysed by considering horizontally periodic modes with wavenumber k. Observe that the perturbed equations would contain time derivatives arising from (2.1) and the kinematic condition, (2.3). A term with two derivatives in time therefore arises from the perturbed pressure field using (2.5), but the appearance of $\cos \omega t$ via the base pressure gradient prevents us from expressing the state variables in pure exponential time modes. Instead the periodicity of the system must be taken into account by including a Floquet exponent, σ, possibly complex, in the infinite Fourier series. The Fourier series is written in modes of the basic frequency, ω, for convenience. Accounting for both the horizontal spatial and temporal dependence of

https://doi.org/10.1017/jfm.2013.324 Published online by Cambridge University Press

the system, for every dependent variable, ψ, we write

$$\psi = \mathrm{e}^{\mathrm{i}\boldsymbol{k}\cdot\boldsymbol{r}} \sum_{n=-\infty}^{\infty} \mathrm{e}^{[\sigma+\mathrm{i}(\alpha+n\omega)]t} \hat{\psi}_n(z). \tag{2.6}$$

To evaluate the z-derivatives of w in (2.5), the velocity profile must be calculated. After elimination of pressure from the linearized equations of motion and substituting (2.6) into them and dropping the $\hat{}$, the fourth-order ordinary differential equation governing each Fourier mode, n, for w is

$$[\sigma + \mathrm{i}(\alpha + n\omega) - \nu_j(\partial_{zz} - k^2)](\partial_{zz} - k^2)w_{jn} = 0, \tag{2.7}$$

to which the solutions are

$$w_{jn} = a_{jn}\mathrm{e}^{kz} + b_{jn}\mathrm{e}^{-kz} + c_{jn}\mathrm{e}^{q_{jn}z} + d_{jn}\mathrm{e}^{-q_{jn}z} \tag{2.8}$$

with

$$q_{jn}^2 = k^2 + \frac{\sigma + \mathrm{i}(\alpha + n\omega)}{\nu_j} \tag{2.9}$$

where ν is the kinematic viscosity. In the case of $\sigma + \mathrm{i}(\alpha + n\omega) = 0$ the functions containing q_{jn} are replaced with $z\mathrm{e}^{kz}$. The boundary conditions determine the coefficients in (2.8). The no-slip boundary conditions on the bottom and top surfaces are

$$w_{1n} = \partial_z w_{1n} = 0 \quad \text{at } z = -h_1, \tag{2.10a}$$

$$w_{2n} = \partial_z w_{2n} = 0 \quad \text{at } z = h_2, \tag{2.10b}$$

and at the interface $z = 0$ we have

$$w_{1n} = w_{2n}, \tag{2.11}$$

$$\partial_z w_{1n} = \partial_z w_{2n}, \tag{2.12}$$

$$\mu_1(\partial_{zz} + k^2)w_{1n} = \mu_2(\partial_{zz} + k^2)w_{2n}, \tag{2.13}$$

and

$$w_{1n} = w_{2n} = (\sigma + \mathrm{i}(\alpha + n\omega))\zeta_n. \tag{2.14}$$

The pressure p in 2.5 can be replaced with an expression including the vertical velocity component w using the x and y components of the perturbed equations of motion along with continuity. The final form of the normal component of the stress balance for each Fourier mode is

$$[[(\rho_j(\sigma + \mathrm{i}(\alpha + n\omega)) + 3\mu_j k^2)\partial_z w_n - \mu_j \partial_{zzz} w_n]] + (\Delta\rho g - \gamma k^2)k^2\zeta_n$$
$$= A\omega^2 \frac{\Delta\rho k^2}{2}(\zeta_{n+1} + \zeta_{n-1}). \tag{2.15}$$

Here $\Delta\rho = \rho_2 - \rho_1$ is used. The identity $\cos\omega t = (\mathrm{e}^{\mathrm{i}\omega t} + \mathrm{e}^{-\mathrm{i}\omega t})/2$ has also been used, resulting in the coupling of the nth Fourier mode ζ_n to the $n+1$ and $n-1$ modes. The linear stability of the system is solely governed by the infinite series of equations given by (2.15), and substitution of the derivatives calculated from (2.8) gives a series of coupled linear equations homogeneous in ζ_n. The series of equations are truncated to a finite number of modes, N, with the growth constant, σ set to zero. The linearized problem can then be cast as an eigenvalue problem to obtain the solutions for neutral

https://doi.org/10.1017/jfm.2013.324 Published online by Cambridge University Press

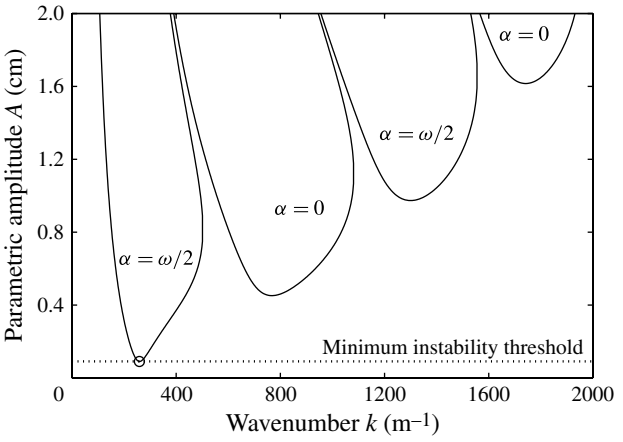


FIGURE 1. Linear stability threshold for a horizontally infinite bilayer of FC70 (1880 kg m^{-3}, 12 cSt) and silicone oil (846 kg m^{-3}, 1.5 cSt) with $h_1 = h_2 = 0.5$ cm, and frequency $f = \omega/2\pi = 9$ Hz. Interfacial tension estimated to be 7 dyn cm^{-1} (Someya & Munakata 2005).

stability. The eigenvalues are the amplitudes, A, and the eigenvalue problem takes the form

$$\boldsymbol{D\zeta} = A\boldsymbol{B\zeta}. \tag{2.16}$$

Here the matrix $\boldsymbol{D}$ is generated by the left-hand side of (2.15) and operates on the eigenvector $\boldsymbol{\zeta}$. The response frequency α is set to zero in (2.15) for harmonic solutions and to $\omega/2$ for subharmonic solutions. The matrix $\boldsymbol{B}$ has two non-zero diagonals, which couples the modes ζ_n, but differs slightly for the $n = 0$ mode. Truncation from $n = 0$ to N results in the inclusion of the ζ_{-1} coefficient in the matrix $\boldsymbol{B}$ for the $n = 0$ mode, and is replaced with the conjugate $\overline{\zeta_1}$ for $\alpha = 0$ and $\overline{\zeta_0}$ for $\alpha = \omega/2$, to ensure reality of the expansion (2.6). The solution of (2.16) yields a set of eigenvalues, A, for which the lowest real eigenvalue corresponds to the first excited mode in a physical system when the forcing amplitude is gradually increased from zero upward.

Solving the linearized problem for all wavenumbers k yields a set of tongues of instability similar to the fins produced by the Mathieu equation (Benjamin & Ursell 1954), but with the tips smoothed by viscosity and not descending to zero amplitude: see figure 1. For these calculations N was taken to be 12. The linear system response arising from these tongues alternates between subharmonic ($\alpha = \omega/2$) and harmonic ($\alpha = 0$), where the first tongue is subharmonic. We refer to the first tongue as subharmonic, the second as harmonic, and the third as superharmonic, as the waves excited in these regions execute one-half, one, and one-and-a-half periods per cell period, respectively. In an experimental system that approaches the laterally infinite limit, such as that of Bechhoefer *et al.* (1995), the wavenumber with the lowest threshold amplitude would be excited first in a series of trials of increasing vibrational amplitudes. In figure 1 the minimum threshold occurs at $A = 0.104$ cm with a wavenumber k of 258.1 m^{-1}. The first excited mode, typically, is a subharmonic mode in the first tongue, but it has been seen that lowering a fluid layer height can result in a bicritical amplitude where modes in the first harmonic and subharmonic tongues can be excited simultaneously. Further lowering of the height excites the harmonic mode (Kumar 1996). The harmonic response with a thin layer was confirmed experimentally by Müller *et al.* (1997), and a nonlinear pattern-forming

https://doi.org/10.1017/jfm.2013.324 Published online by Cambridge University Press

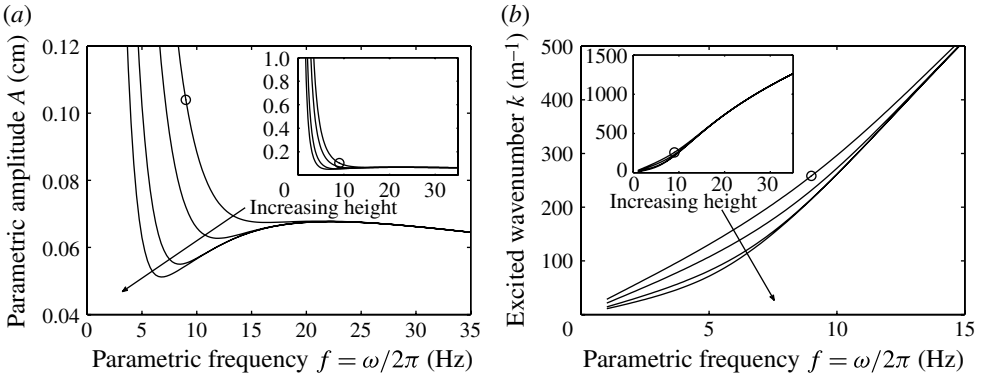


FIGURE 2. Frequency-dependent predictions for (*a*) threshold amplitude and (*b*) wavenumber selection for FC70–silicone oil bilayers of $h_1 = h_2 = 0.5$, 0.75, 1.5 and 2.5 cm. Physical parameters are the same as in figure 1. Circled point denotes the first excited mode from figure 1. Hereon, frequency and amplitude denote the parametric conditions, unless otherwise noted.

study near the co-dimension 2 point was done by Wagner, Müller & Knorr (2003). The theoretical curve matched by Bechhoefer *et al.* (1995) can be generated by calculating the minimum point in figure 1 for a range of frequencies, noting that their curves depict forcing acceleration, $A\omega^2$, instead of forcing amplitude, A. An example of this calculation is given in figure 2(*a*) for several different layer heights, while the corresponding wavenumber selection is shown in figure 2(*b*). It can be seen that the general behaviour of these curves depends upon the layer height. At low forcing frequency the minimum threshold increases without bound as the frequency is decreased, agreeing with intuition that a light over heavy system is stable. Increasing the forcing frequency causes a sharp drop in the minimum threshold amplitude. For the systems of large layer height the threshold can drop to a minimum value before rising and then dropping again. The wavenumber selection in figure 2(*b*) shows that for lower layer heights, the selected wavenumber is higher. The shift toward higher wavenumbers arises from a diminished gravitational effect when the layer heights are small. We note that resonance is obtained on account of a gravitational as well as capillary contribution. It is therefore apparent that a reduced gravitational effect leads to a greater capillary contribution. Higher wavenumbers are associated with greater viscous effects and this is seen in the rises in the threshold present in the systems of $h_1 = h_2 = 1$, 1.5 and 2.5 cm in figure 2(*a*). For the $h_1 = h_2 = 0.75$ cm case, the height is sufficiently low such that the viscous effects are important at much lower frequencies than in the other cases, and a local minimum in the threshold curve is therefore barely seen.

2.2. *Spatially finite systems*

Extension of this model to the case of a cell with finite lateral dimension that permits separation of horizontal cell modes was outlined by Benjamin & Ursell (1954) for both rectangular and cylindrical cross-sections. They applied these conditions to their stability results generated by the Mathieu equation, and the application to the viscous model is much the same. For the case of a cylinder of radius R, the allowed eigenfunctions $\zeta_m = \zeta(r, \theta)$, which are compatible to the stress-free condition on the

https://doi.org/10.1017/jfm.2013.324 Published online by Cambridge University Press

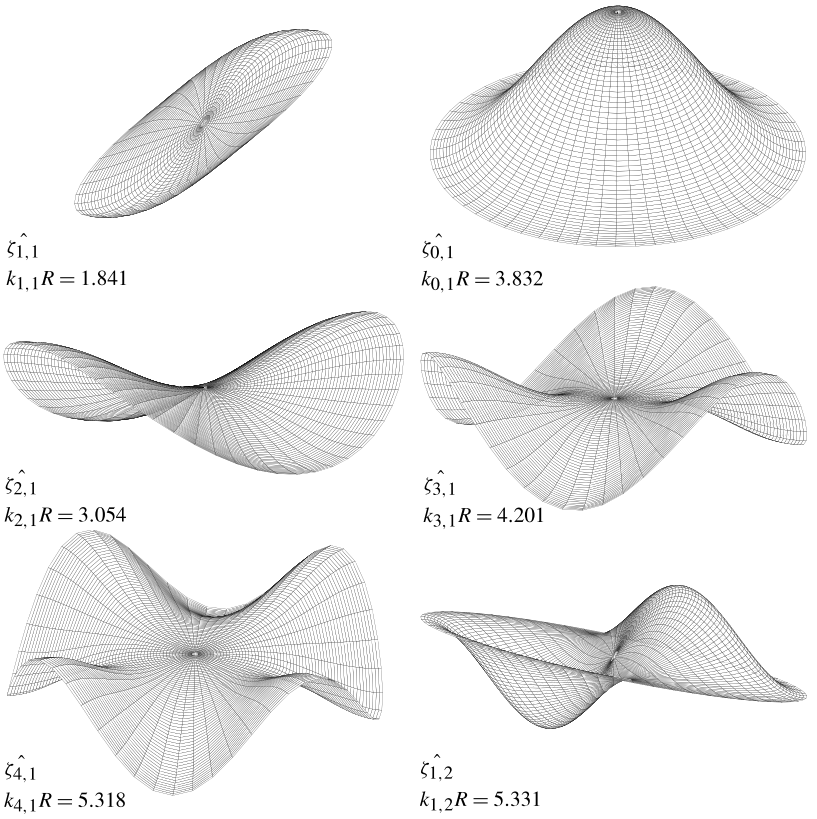


FIGURE 3. Spatial forms and dimensionless wavenumbers of various cylindrical cell modes satisfying the stress-free boundary condition.

vertical walls, are given by the functions satisfying

$$\left(\frac{\partial^2}{\partial r^2} + \frac{1}{r}\frac{\partial}{\partial r} + \frac{1}{r^2}\frac{\partial}{\partial \theta} + k_m^2\right)\zeta_m = 0, \tag{2.17}$$

which can then be decomposed as

$$\zeta_m = \mathrm{J}_l(k_{l,m}r)\sin l\theta\hat{\zeta}_{l,m}, \tag{2.18}$$

where $k_{l,m}$ is the mth zero of $\mathrm{J}_l'(k_{l,m}R)$. The indices l and m indicate the number of azimuthal and radial nodes, respectively. The spatial forms and non-dimensionalized values $k_{l,m}R$ of various cylindrical linear modes $\zeta_{l,m}$, are presented in figure 3 (Abramowitz & Stegun 1964).

The critical thresholds corresponding to these allowed modes (in addition to higher index modes) have been labelled on stability diagrams of two different frequencies in figure 4(*a*,*b*). Here it is apparent that the wavenumber corresponding to the subharmonic minimum threshold is excited only in the case where it coincides with one of the allowed modes. Harmonic and superharmonic excitation is uncommon at high frequencies, but at low frequencies in a discretized system one can possibly skip the first subharmonic tongue and excite harmonic and superharmonic modes, as in figure 4(*a*), where the $(2, 1)_h$ mode would be excited first at an amplitude of 0.92 cm.

https://doi.org/10.1017/jfm.2013.324 Published online by Cambridge University Press

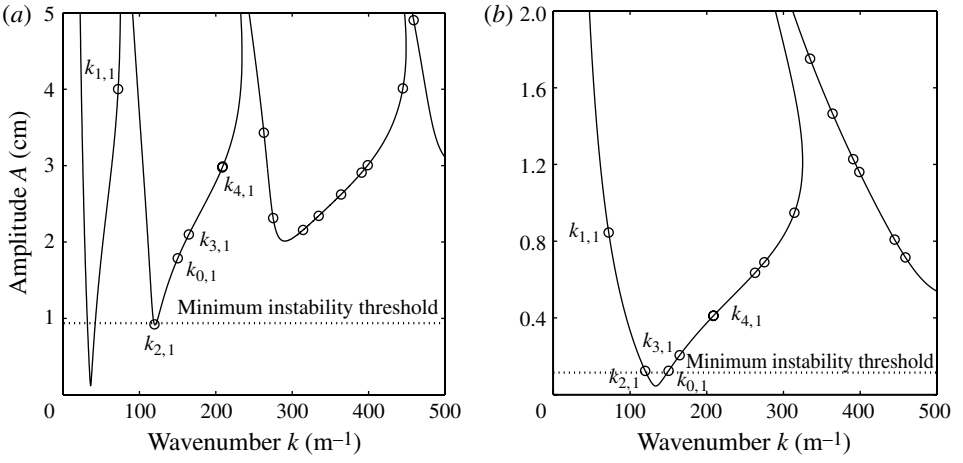


FIGURE 4. Predictions for an FC70–silicone oil bilayer of $h_1 = 3.1$ cm and $h_2 = 3.3$ cm contained in a cylinder of $R = 2.55$ cm at frequencies (*a*) 3.3 Hz and (*b*) 7.045 Hz. Physical parameters are the same as in figure 1.

The stability diagram of figure 4(*b*) was calculated for a carefully chosen frequency to highlight the appearance of a co-dimension 2 point, a set of conditions where two modes are both neutrally stable for the same amplitude and frequency. Here, both $(2, 1)_{sh}$ and $(0, 1)_{sh}$ modes are simultaneously excited at an amplitude of 0.123 cm.

Figure 5 shows all of the previously discussed aspects of discretization, where the minimum amplitudes of instability from calculations such as figure 4 are plotted versus a multitude of frequencies for a cylindrical system. The figure depicts the overlapping dips of instability for each mode, descending to minimum thresholds. Each dip corresponds to a single-mode $\zeta_{l,m}$ specified by (2.18). When positioned at one of the local minima, slight adjustment to a lower or higher frequency causes the threshold to rise as the resonant transfer of energy to the wave becomes less efficient. The modes excited at frequencies higher than the minima are referred to as tuned modes, and those at lower frequencies as detuned modes. This distinction is important because Benjamin & Ursell and many others have noted different nonlinear behaviour near the threshold for tuned and detuned modes, which will be discussed later in the context of determining the experimental threshold. Further departure from a local minimum results in the intersection with an adjacent mode. These intersections, or cusps, are the co-dimension 2 points highlighted by figure 5. The general ordering of the modes is dictated by the wavenumber, where at low frequencies harmonic and superharmonic modes are prevalent, followed by subharmonic modes at the higher range. The physical parameters used to calculate figure 5 are the same as in one of the experiments of this study, and one result of this is the viscous damping of sharp resonances at low frequencies entering from the higher harmonic tongues. One of the benefits of using a viscous system is a series of well-spaced modes, resulting from the damping of resonances with the harmonic and superharmonic tongues. It will be shown in the next section that the use of less viscous systems, typical of previous work, makes individual modes more difficult to discern due to the appearance of sharp resonances with these tongues. The infinite system threshold, depicted by a dashed line, is included for comparison in figure 5; its origin is figure 2(*a*). At large

https://doi.org/10.1017/jfm.2013.324 Published online by Cambridge University Press

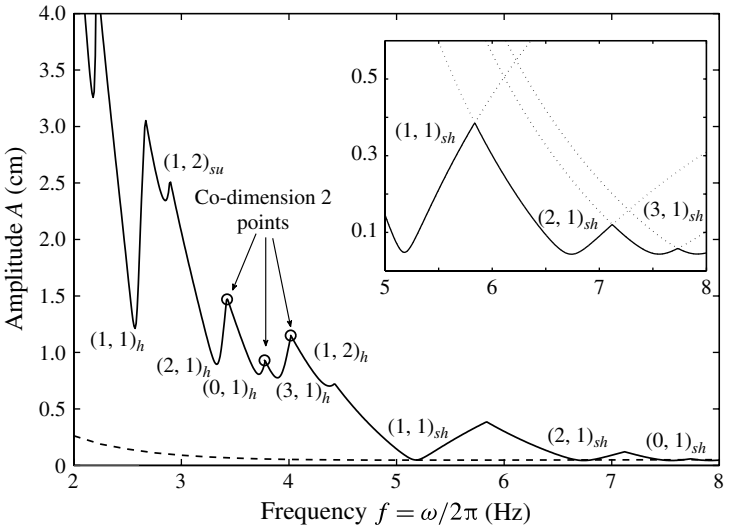


FIGURE 5. Linear threshold predictions for a bilayer of FC70 (1916 kg m^{-3}, 12 cSt, $h_1 = 3.1$ cm) and silicone oil (846 kg m^{-3}, 1.5 cSt, $h_2 = 3.3$ cm) in both an infinite system (dashed line) and cylindrical $R = 2.55$ cm system. Subscripts *sh*, *h* and *su* represent subharmonic, harmonic, and superharmonic modes.

frequencies the finite system threshold is very nearly identical to the infinite threshold, and continued increase in frequency causes the merging of the two.

These predictions constitute a model for single-mode excitation in which dissipation arises only from the interior, and what will now be shown is that prior single-mode experiments do not satisfy the ideality of this model, thereby providing motivation for the current work.

3. Previous experiments in small cylinders

One of the central purposes of this work is to reproduce the thresholds predicted in figure 5. Several Faraday experiments were performed in small cylinders with the aim of measuring the onset of instability, in the regime where mode discretization is important. Most often the experiments investigated the stability boundary for only one or two modes in a system with limited interior viscous effects. In contrast large dissipation arising from the sidewalls results in systems exhibiting non-ideal behaviour. Comparison of the data from these experiments to the predictions of the Kumar & Tuckerman model highlights many of the discrepancies in previous experiments, to which the current study will provide new insight. In figure 6(*a–f*) the results of these works have been compared to this model and will be discussed.

The early experiments of Benjamin & Ursell (figure 6*a*) utilized a deep layer of water as the operating fluid in a test cylinder of diameter 5.4 cm. Using the nodal indexing of this work, they investigated the $(1, 2)_{sh}$ mode, appearing with a natural frequency at 15.82 Hz, in contrast to the inviscid natural frequency of 15.87 Hz. Respectable agreement with their inviscid model was found after shifting the natural frequency to the observed frequency, but the amplitudes are noticeably higher at the tongue minimum, a result of system dissipation. Upon fitting the data with the viscous model, it is seen that the stability tongue is modified only slightly, indicating that the

https://doi.org/10.1017/jfm.2013.324 Published online by Cambridge University Press

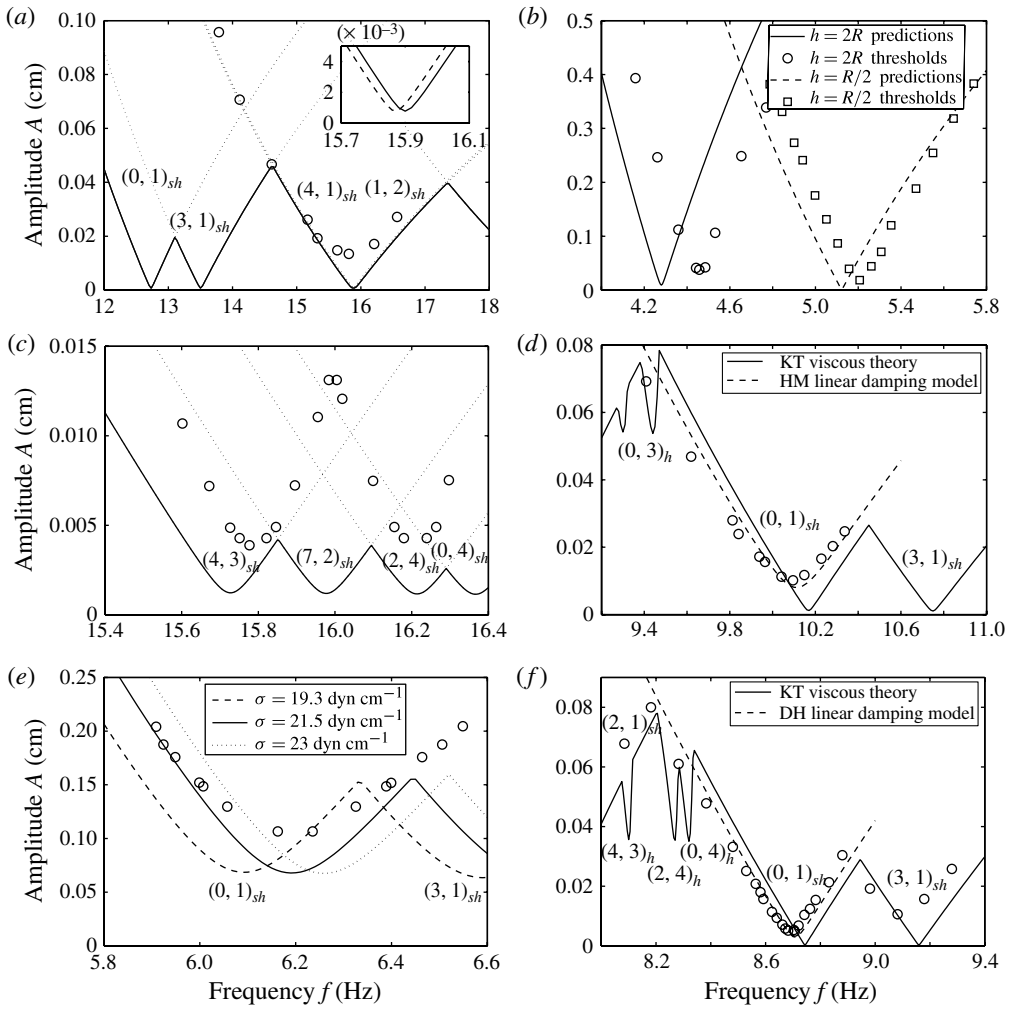


FIGURE 6. Past experimental threshold data and viscous model predictions for: (*a*) Benjamin & Ursell (1954), water and air, $\rho = 1000\ \mathrm{kg\ m^{-3}}$, $\nu = 1$ cSt, $\gamma = 72.5\ \mathrm{dyn\ cm^{-1}}$, $R = 2.70$ cm, $h = 25.4$ cm; (*b*) Dodge, Kana & Abramson (1965), water and air, $R = 14.5$, $h = 29$ and 7.25; (*c*) Ciliberto & Gollub (1985), water and air, $R = 6.35$, $h = 1$; (*d*) Henderson & Miles (1990), water/surfactant and air, $\gamma = 42.3$, $R = 3.725$, $h = 2.04$; (*e*) Tipton & Mullin (2004), water and silicone oil, $\rho_1 = 997.5$ and $\rho_2 = 766$, $\nu_1 = 1.033$ and $\nu_2 = 0.670$, γ unreported and set to 21.5, $R = 1.76$, $h_1 = 5.31$ and $h_2 = 0.739$; (*f*) Das & Hopfinger (2008), FC72 and air, $\rho = 1690$, $\nu = 0.406$, $\gamma = 11$, $R = 5$, $h = 6$. All theoretical comparisons are made to the model of Kumar & Tuckerman (1994), assuming stress-free sidewalls and no interfacial dissipative effects. The dashed lines in figures (*d*,*f*), however, are the linear damping predictions of the original works and are reproduced here for comparison to the case of stress-free sidewalls. All units are the same as listed for (*a*).

viscous contribution of the interior is negligible. One therefore can only conclude that the hidden dissipation comes from either sidewall or from interfacial dissipative effects. A finding of the current work is that experimental agreement with the theory improved

https://doi.org/10.1017/jfm.2013.324 Published online by Cambridge University Press

with the increase of the Bond number

$$Bo = \frac{\Delta\rho g}{\gamma k^2}, \tag{3.1}$$

a measure of the relative importance of the capillary effects. For the experiments of Benjamin & Ursell, the Bond number was 3.47. Careful inspection of all the predictions shows that the $(4, 1)_{sh}$ mode occupies nearly the same stability space as that of the $(1, 2)_{sh}$ mode, which is explained by noting that the dimensionless wavenumbers $k_{41}R$ and $k_{12}R$ are identical to each other within 1 % (see figure 3). Therefore the selection of the $(1, 2)_{sh}$ mode in the experiment is an important observation to make and we will present arguments later that this is a result of sidewall effects. Also, the first two data points fall well inside the region of instability for the $(3, 1)_{sh}$ and $(0, 1)_{sh}$ modes, but these modes have apparently been damped entirely and instead the $(1, 2)_{sh}$ mode remains.

Dodge *et al.* (1965) ran experiments, also using water, in a cylinder with a rather large diameter of 14.5 cm, measuring critical thresholds and wave amplitudes. Figure 6(*b*) shows their onset measurements for the $(1, 1)_{sh}$ mode for two different layer heights, along with the predicted viscous thresholds. Their thresholds observed better agreement at the tongue minima than that of Benjamin & Ursell, probably due to the large tank dimensions and the relatively smaller sidewall contribution to the overall dissipation. A quantitative indicator is the Bond number of 839, which is the largest of all the previous experiments. However, as acknowledged by Dodge *et al.*, the shifting of the experimental natural frequencies to higher frequencies is surprising. This is in contrast to the shift toward lower frequencies, observed by Benjamin & Ursell. Notably, the frequency bandwidths of 0.5 and 0.9 Hz were rather small, in part due to the large tank dimensions. A shift toward higher frequencies (and amplitudes) than predicted is also encountered with the thresholds of Ciliberto & Gollub (1985) (figure 6*c*, $Bo = 3.39$), who explored chaotic behaviour near the co-dimension 2 point of a $(4, 3)_{sh}$ and a $(7, 2)_{sh}$ mode. Their frequency bandwidths of 0.4 and 0.3 Hz were also notably small. Comparison of the predictions for the systems of Dodge *et al.* (1965) and Ciliberto & Gollub (1985) also illustrates how the viscous damping of the thresholds can differ for systems of the same working fluid when the heights and mode are different.

Of great significance are the experiments of Henderson & Miles (1990), who made the first attempt at matching single-mode experiments to a theory incorporating viscous effects. Henderson & Miles performed experiments in a $R = 3.725$ cm cylindrical cell with water as the operating fluid, using a surfactant to minimize the pinning of the interface to the sidewalls. Viscous damping was modelled using the theory of Miles (1967), assuming that the effects were constrained to laminar boundary layers along the interface and the sidewalls. However, in the damping model, the water viscosity had to be taken to be 3 cSt to produce the experimentally observed damping rates in the cylinder. Nonetheless, incorporation of this damping rate into the model for the thresholds produced respectable agreement with the experiment for the $(0, 1)_{sh}$ mode in the cylinder. The negative shift in the observed natural frequency was accounted for, as was the damping of the thresholds. The predictions of this linear damping model and their data are reproduced alongside the predictions of the viscous model in figure 6(*d*). In comparison, it is seen that the region of instability is only slightly damped for the viscous theory, much like the systems of Benjamin & Ursell and Dodge *et al.*, implying that again bulk viscous effects were not the primary source of damping in these experiments. The linear damping coefficient due to viscous effects

https://doi.org/10.1017/jfm.2013.324 Published online by Cambridge University Press

in the bulk phases, given by Kumar & Tuckerman (1994) and derived by Landau & Lifshitz (1987), ignoring interfacial effects, is given by

$$\gamma_{visc} = 2k^2 \frac{\mu_1 \coth kh_1 + \mu_2 \coth kh_2}{\rho_1 \coth kh_1 + \rho_2 \coth kh_2}. \tag{3.2}$$

It follows that the linear contribution to the bulk viscous effect in these experiments was $\gamma_{visc} = 0.0216\ \mathrm{s}^{-1}$, only $\sim 5\,\%$ of the measured damping rate of $0.44\ \mathrm{s}^{-1}$, implying that the system's dissipation was dominated by the wall and interfacial dissipative effects. The frequency shift and slight deviation of the $(0, 1)_{sh}$ thresholds in the work of Henderson & Miles (1990) ($Bo = 21.9$) is also seen in the experiments of Das & Hopfinger (2008), who also measured the threshold of the $(0, 1)_{sh}$ mode, but in a large $R = 5$ cm cell ($Bo = 257$). Figure 6(f) reveals the deviation of the data from the viscous model to be qualitatively the same although arguably less than that of Henderson & Miles for both the $(0, 1)_{sh}$ mode and its neighbouring $(3, 1)_{sh}$ mode. Negative frequency shifts were observed along with threshold damping. The damping of the tuned $(3, 1)_{sh}$ thresholds appears to be greater than the tuned thresholds of the $(0, 1)_{sh}$ mode, a result consistent with the findings of our experiments.

Other experiments of note are those of Ito, Tsuji & Kukita (1999) and Tipton & Mullin (2004), because, like the experiments in this work, both were run for liquid bilayers as opposed to a liquid with a passive air layer. The experiments of Ito *et al.* are qualitatively different from traditional single-mode experiments, as they were interested in modelling the effect of sidewall flow perturbations on the instability. In their experiment, a column of water with kerosene lying on top of it was pumped in an oscillatory manner using a piston, producing a moving interface like the Faraday problem. However, base flow perturbations arose from shear flows at the sidewalls. They observed the growing cell modes at different frequencies much like the Faraday experiment, but in general the data do not agree with the viscous Faraday model and are not shown here. Of note, however, are the observations by Ito *et al.* of the development of a film produced by kerosene on the sidewalls. Qualitatively, this film was the same as observed in this work, and Ito *et al.* provide excellent discussion of its dynamics. Additionally, Ito & Kukita (2008) further study the effect of the film on the nonlinear dynamics of the instability.

Tipton & Mullin (2004) probed the bifurcation structure of the $(0, 1)_{sh}$ mode in a closed stainless steel cylinder containing water and silicone oil for a variety of liquid heights, and observed a non-dimensionalized collapse to the predictions of a linearly damped Mathieu equation. They noted that their damping parameter was eight times the value predicted by (3.2), suggesting that wall effects were important in their cell. The interfacial tension between their oil and water was also not measured, requiring guesses to be made to fit the viscous model to their data. Due to the small density difference between water and oil, this system stands out for being the only set of previous experiments where the surface tension made a significant contribution to the mode dispersion. Taking the interfacial tension to be $21.5\ \mathrm{dyn\ cm}^{-1}$, a match can be made between the observed and predicted natural frequencies, but is lost when the value is adjusted slightly. At an interfacial tension of around $19\ \mathrm{dyn\ cm}^{-1}$ (a value suggested in private communication with Tipton & Mullin), the discrepancy is significant: see figure 6. It appears that the thresholds lay above the viscous prediction regardless of the exact value chosen, and the cell diameter of 35.22 mm, the smallest of the reviewed experiments, suggests that the dissipation due to wall effects was controlling. Additionally, the Bond number here of 2.4 was the lowest of all of the reviewed experiments.

https://doi.org/10.1017/jfm.2013.324 Published online by Cambridge University Press

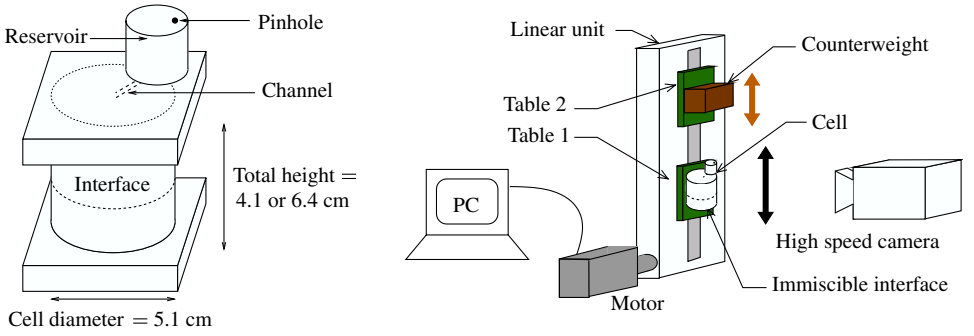


FIGURE 7. (Colour online) Test cell and the electromechanical shaker.

Application of the viscous model to the past results clearly shows that there have been many experimental unknowns which are not accounted for in the linear stability model. This has resulted in different forms of mismatch between experiments and theory, including mode shifts toward both higher and lower frequencies, increases in the threshold amplitudes and the complete absence of predicted modes. Broader interpretation of these systems cannot be given due to the limited scope of these studies, often limited to only one or two modes. Thus, in addition to a better replication of the assumptions of the linear theory, another important goal of this work is to study an entire range of modes, as presented in figure 5, where the interaction between the sidewall and the instability can be more deeply understood.

4. Experimental method

Experiments were performed using an electromechanical shaker capable of independent adjustment of frequency and amplitude, producing maximum accelerations of $3g$ at frequencies of up to 15 Hz. All cell and interfacial motion were examined using time–space data of the images, obtained from high speed digital imaging with frame rates of up to 2000 fps. Fourier transform analysis of the cell motion determined the frequency control to be precise to within 0.1 % of the setpoint. Accuracy in the imposed vibrational amplitude was estimated to be better than 1 % and interface deflection amplitude was estimated to be comparable, albeit slightly less precise due to optical bending through the cell.

The experimental cell was constructed with two Plexiglas plates with machined trenches to produce an o-ring seal at the ends of glass cylinders of $R = 2.55$ cm producing two effective heights of 4.1 and 6.4 cm. To prevent leaks or bubble generation caused by thermal effects, a 1 mm channel in the top plate was connected to an external reservoir into which the cell fluid could either expand or contract: see figure 7. Perturbations due to flow into or out of the channel were assumed to be insignificant, and this allowed the creation of a completely filled system with which experiments could be run continuously over the course of weeks. A square cage was built around the cell with thin Plexiglas plates and filled with water to improve the optics of the cell wave motion. The external cell motion was tracked using marks made on the cell exterior.

Experiments were performed with 3M^{TM} Fluorinert electronic fluid FC70 ($\nu =$ 12 cSt) and silicone oils. Densities were measured using a pycnometer with a calibrated volume of 51.490 mL. The density of FC70, listed as 1940 kg m^{-3}, was

https://doi.org/10.1017/jfm.2013.324 Published online by Cambridge University Press

found to vary from bottle to bottle, and therefore the density used for theoretical predictions is noted with the figures. Silicone oils of 10 cSt ($\rho = 944$ kg m^{-3}) and 1.5 cSt ($\rho = 846$ kg m^{-3}) were used. A lower viscosity silicone oil of 0.65 cSt was removed from consideration because it was found to be slightly miscible with FC70. The density difference between the two phases plays a large role in the positioning of the thresholds in the discretized regime, considering that the excited modes are primarily gravity waves with little capillary contribution. The range of frequencies for which discretization is important increases for a system with larger density difference, since the wavenumber selected is always lower and the same mode appears at higher frequencies. At low frequencies the instability threshold is also lowered for large density differences, meaning that harmonic and superharmonic modes are more easily accessed. The density difference in these experiments of nearly 1000 kg m^{-3} is quite similar to a water and air system, but the difference in behaviour is different considering the higher viscosities.

It was found that FC70 and silicone oils produced a nearly flat interface with only a slight meniscus (less than 1 mm). Upon tilting of the filled cell, the interface was seen to move with great ease along the sidewalls in contrast to the sluggish interface between oil and water, which exhibits stick–slip-type behaviour, even when different wetting agents were applied to the sidewalls. Neither viscosities nor interfacial tensions were measured. Slight adjustment of viscosity above or below the assumed values has very little effect on the predicted threshold curves. Additionally, interfacial tension shows virtually no effect on the theoretical predictions, as the large density difference between FC70 and silicone oils dominates the capillary contribution in the considered frequencies. Interfacial tension between FC70 and silicone oil is estimated to be 7 dyn cm^{-1} (Someya & Munakata 2005).

A valuable and common measurement in the single-mode experiments is the rate at which an excited mode decays once the excitation has been stopped. These damping rates can be used to model the dynamics as a single degree of freedom system, first done by Henderson & Miles (1990). However, in the case of the experiments in this study the rates will primarily be used to gauge the amount of dissipation in the system due to bulk viscous effects not included in (3.2). The exponential rate of decay is determined by the slope of the logarithm of the ratio of the wave amplitude scaled by the initial value plotted against time. This was done for both harmonic and subharmonic (0, 1) modes, for which the maximum wave height occurs at the z-axis. Imaging of the mode and selection of the time space of this central position produces a decay. The wave amplitude was then measured as half of the difference between the maximum wave amplitude and the apparent contact line. Extensive details on this method can be found in Keulegan (1958) and Henderson & Miles (1990) and Das & Hopfinger (2008).

5. Results of experiments

5.1. *Sidewall behaviour*

The key results are connected to the behaviour of the interface close to the sidewalls, the source of the non-ideality. Filling of the cell with FC70 and silicone oil produced a convex down meniscus in the glass cylinders, a result of the preferential wetting of the glass by the silicone oil. Upon vibration of the cell either below or above the Faraday threshold, the harmonic modulation of the gravity field causes adjustment to the desired meniscus profile, resulting in harmonic emission of an axisymmetric wave from the sidewall. In a system, after the commencement of oscillation, there exists a

https://doi.org/10.1017/jfm.2013.324 Published online by Cambridge University Press

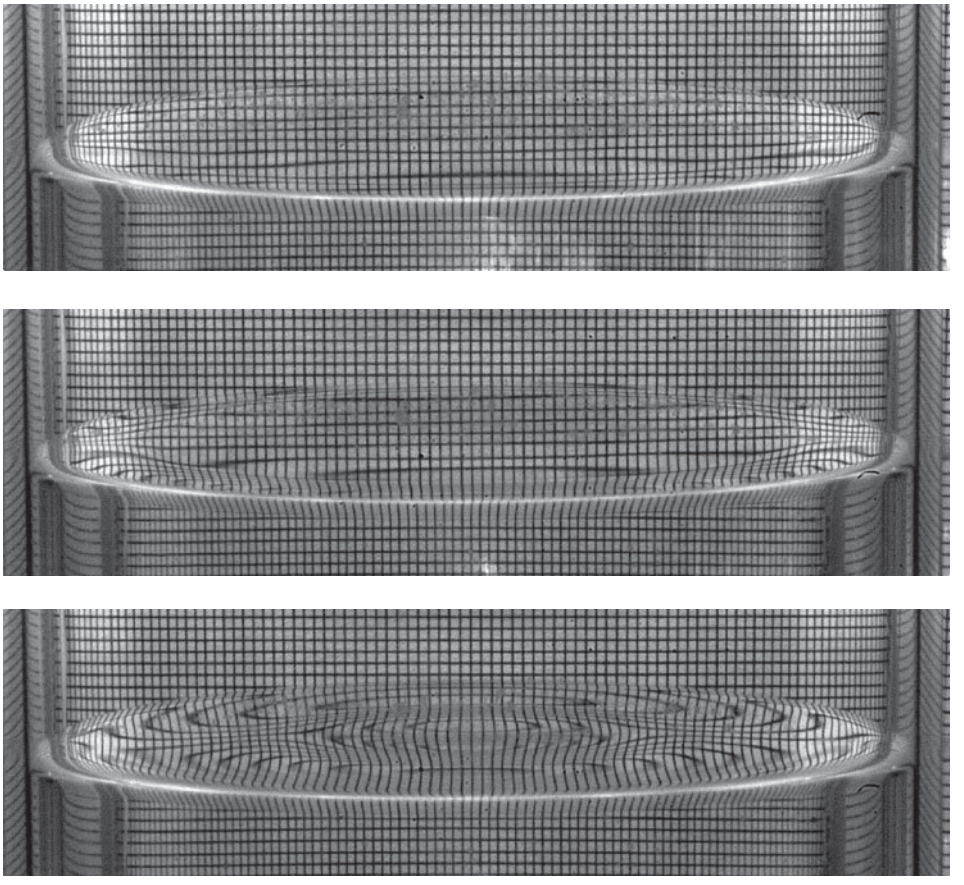


FIGURE 8. Experimental visualization of the static FC70 and 1.5 cSt silicone oil interface and meniscus (*a*), initial meniscus wave emission (*b*), depicted by the bending of the gridlines, and a steady-state meniscus wave profile (*c*). Parametric conditions are 6 Hz and 3.0 mm. The wave profile generated by the meniscus dynamics remains axisymmetric throughout the period of induction prior to growth of the instability. See supplementary movie 1 available at http://dx.doi.org/10.1017/jfm.2013.324.

transient period during which the emission of the meniscus wave and the reflection of the wave through the cylinder's z-axis equilibrates to a steady-state wave that appears as concentric ripples. The quiescent state, initial emission of a wave, and a steady-state meniscus profile are depicted in figure 8. The magnitudes and characteristic wavelengths of these ripples are very much a function of the parametric amplitude and frequency. Finally, although the temporal behaviour of the interior profile is complex due to the persistent emission and reflection of meniscus waves, the alteration of the meniscus remains axisymmetric and harmonically periodic with the cell motion. This periodicity is suspected to interact with the harmonic modes of instability, which will be presented and discussed further on.

Figure 9 depicts the excitation of a $(0, 1)_{sh}$ mode after it has saturated to a steady amplitude. While the nonlinear growth is not the main focus of this work, the transition to this state is essential to be able to reproduce the linear thresholds. The emission of meniscus waves does not alter the contact position of the interface at the

https://doi.org/10.1017/jfm.2013.324 Published online by Cambridge University Press

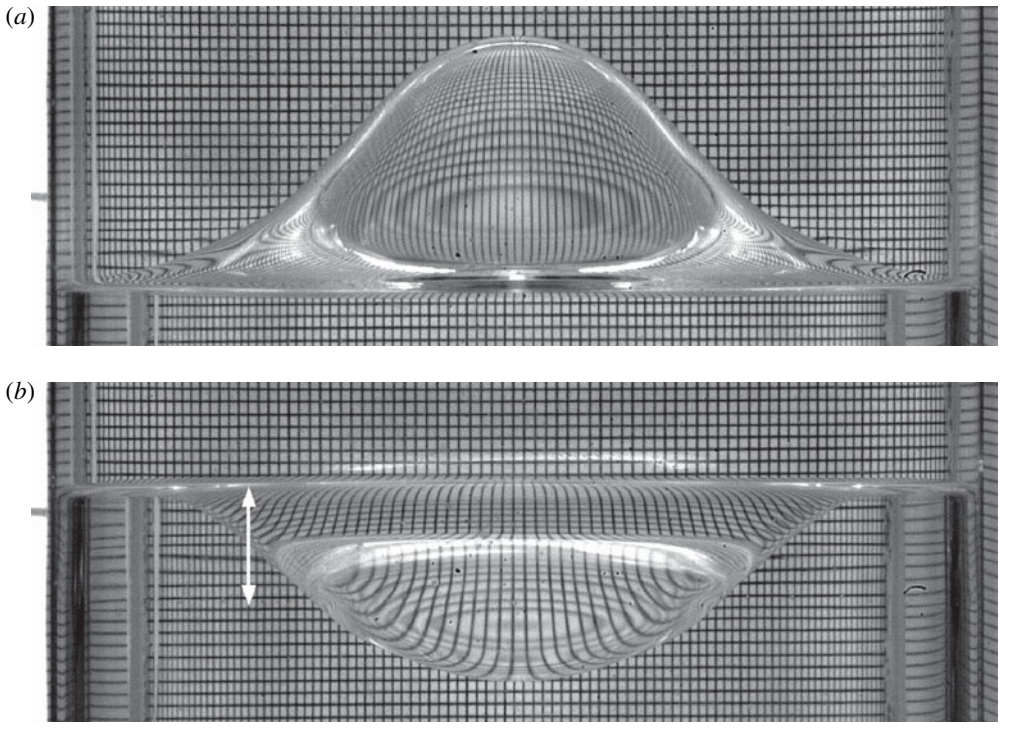


FIGURE 9. Experimental visualization of the excitation of a $(0, 1)_{sh}$ mode for the (*a*) maximum and (*b*) minimum cycle in an FC70 and 1.5 cSt silicone oil system, excited at 7.5 Hz and 1.0 mm. The double-headed white arrow denotes the z-direction difference between the apparent and actual contact lines of the interface. This difference is emphasized in figures 10 and 11, where time series of images of the film dynamics are presented for systems with upper phase viscosities of both 50 and 1.5 cSt. Cell radius $R = 2.55$ cm. See supplementary movie 2.

sidewalls, but excitation of a Faraday wave results in a motion that begins to separate the apparent contact position from the actual position. As the Faraday wave begins to grow, the first downward motion of the interface at the sidewall causes both the apparent and the actual contact line to be pushed downward. For the reverse upward motion of the interface, the apparent contact line moves upward, while the actual contact line remains fixed to the lowest position the interface had reached, as indicated in figure 9. While the actual and apparent contact lines coincide for the upward cycle, the actual contact line lies 0.66 cm below the apparent contact line in the downward cycle, evidenced by the slight optical deformations of the back grid in the far left and right sides of the image. After saturation of the Faraday wave to a finite amplitude, the interface remains tethered to this low position, stretching and contracting vertically as the bulk FC70 glides up and down over a tiny film of silicone oil. This is clearly visualized in figures 10 and 11, with sets of images showing the film dynamics during a period of a saturated $(0, 1)_{sh}$ mode, like figure 9. A system with silicone oil viscosity 50 cSt is shown in figure 10, and the film formation is evidenced by the deformation of the grid as the apparent contact line advances above the pinned position. Temporal asymmetry is seen when the apparent contact line begins to recede, and the profile of the interface more closely represents a 90° angle with the wall. Both the grid

https://doi.org/10.1017/jfm.2013.324 Published online by Cambridge University Press

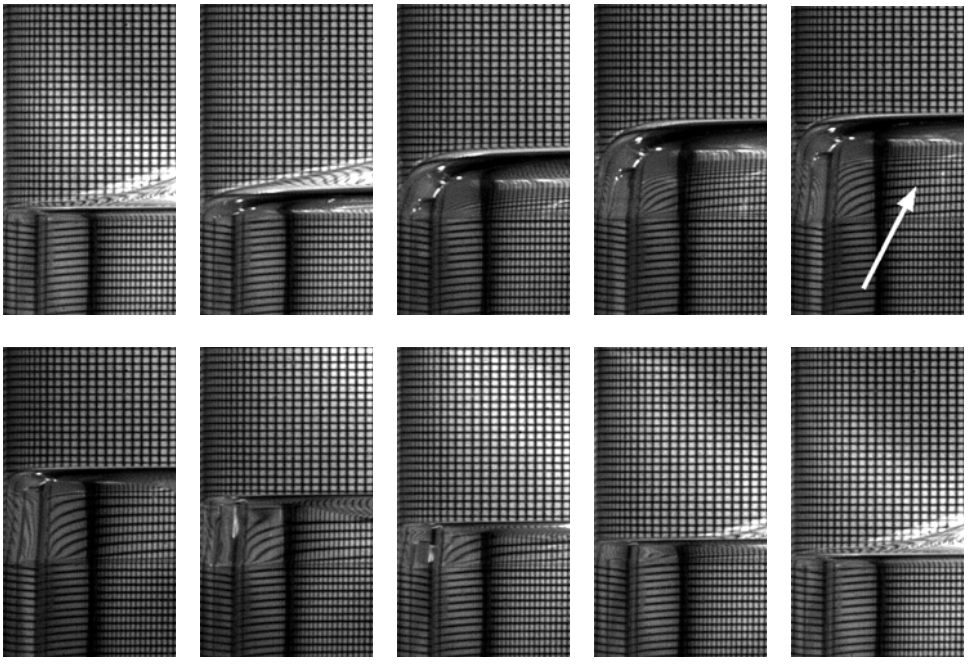


FIGURE 10. Film dynamics for a period of $(0, 1)_{sh}$ motion excited at 6.7 Hz in an FC70 and 50 cSt silicone oil system. The distinction between the apparent and actual contact line is seen moving from left to right and then top to bottom with temporal spacing between each image of 0.299 s. The white arrow focuses on a region where the back grid is most distorted, indicating the presence of a film. Images are presented such that the interface contact line remains constant in each image. See supplementary movie 3.

deformation (film thickness) and asymmetry are more subtle in figure 11, where a set of images has been shown for a $(0, 1)_{sh}$ mode when the upper viscosity is 1.5 cSt. The formation of this film is believed to be critical to the realization of the stress-free boundary condition. Obviously there are stresses introduced through this mechanism, but we shall argue that it is less significant than the viscous stresses arising from bulk fluid motion. The dependence on the upper phase viscosity will be established by first presenting the experimental thresholds for a $(2, 1)_{sh}$ mode when 10 cSt oil is used as the upper phase, followed by the results using 1.5 cSt oil.

5.2. *Experimental thresholds and dependence upon the upper phase viscosity*

Figure 12 presents the experimental onsets of the $(2, 1)_{sh}$ mode and the corresponding theoretical predictions for two FC70–silicone oil systems of identical layer heights in which the upper phase viscosity is (*a*) 10 cSt and (*b*) 1.5 cSt. The data points correspond to sets of conditions at which the instability was observed. A separate experiment performed at an amplitude slightly lower than that of the data points resulted in a system at which the instability did not appear and only the meniscus waves were present. Hysteresis effects have been reported (Benjamin & Ursell 1954; Henderson & Miles 1990; Tipton & Mullin 2004; Das & Hopfinger 2008) on the detuned branch of the curve, where the instability disappears at a frequency or amplitude lower than the onset conditions. This phenomenon, however, was not studied in this work. The end points of the data set correspond to co-dimension

https://doi.org/10.1017/jfm.2013.324 Published online by Cambridge University Press

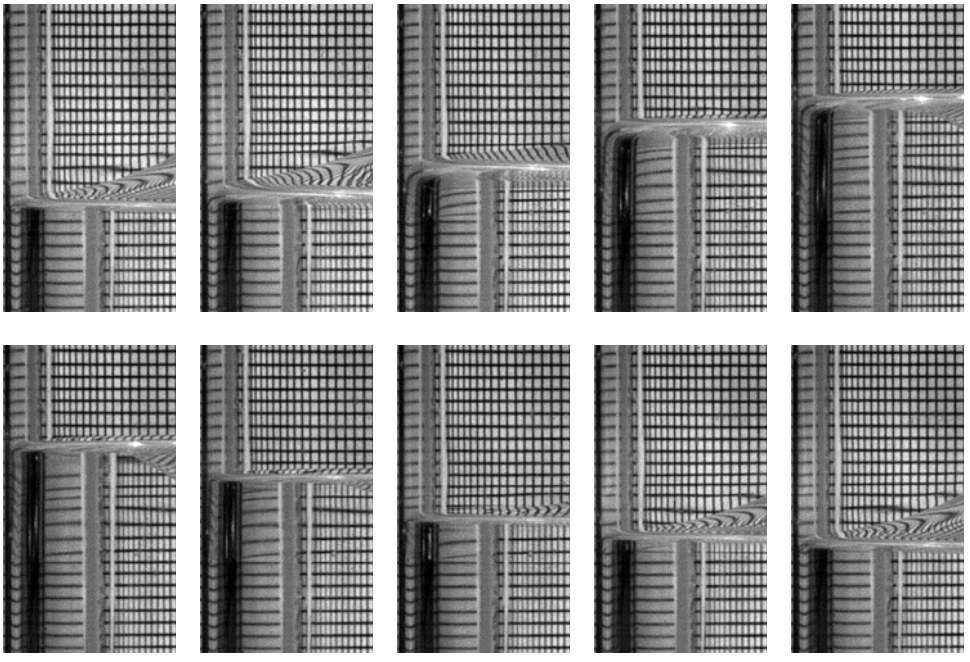


FIGURE 11. Film dynamics for a period of $(0, 1)_{sh}$ motion excited at 7.5 Hz in an FC70 and 1.5 cSt silicone oil system. Moving from left to right and then top to bottom, the temporal spacing between each image is 0.267 s, and the image length scale is the same as figure 9. Images are presented such that the interface contact line remains constant in each image. See supplementary movie 4.

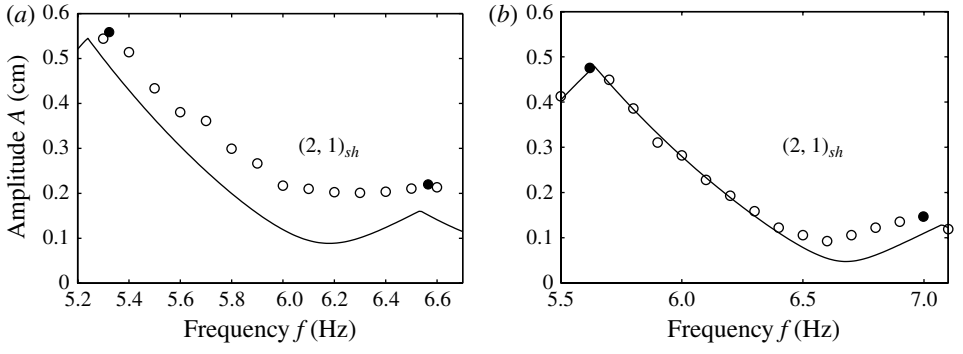


FIGURE 12. Experimental thresholds of and predictions for FC70 (1916 kg m^{-3}) and silicone oil bilayers ($h_1 = 2.1$ cm, $h_2 = 2.0$ cm) in a $R = 2.55$ cm cylinder for (*a*) 10 cSt oil (944 kg m^{-3}) and (*b*) 1.5 cSt oil (846 kg m^{-3}). Open circles represent single-mode thresholds, black dots represent co-dimension 2 points.

2 points: in this case, for both sets of results the left co-dimension 2 point is a superposition of the $(2, 1)_{sh}$ with a $(1, 1)_{sh}$ mode, while the right co-dimension 2 point is a superposition of the $(2, 1)_{sh}$ with $(0, 1)_{sh}$ modes. The latter co-dimension 2 point in the 10 cSt system is visualized in figure 13, exhibiting the same contact line

https://doi.org/10.1017/jfm.2013.324 Published online by Cambridge University Press

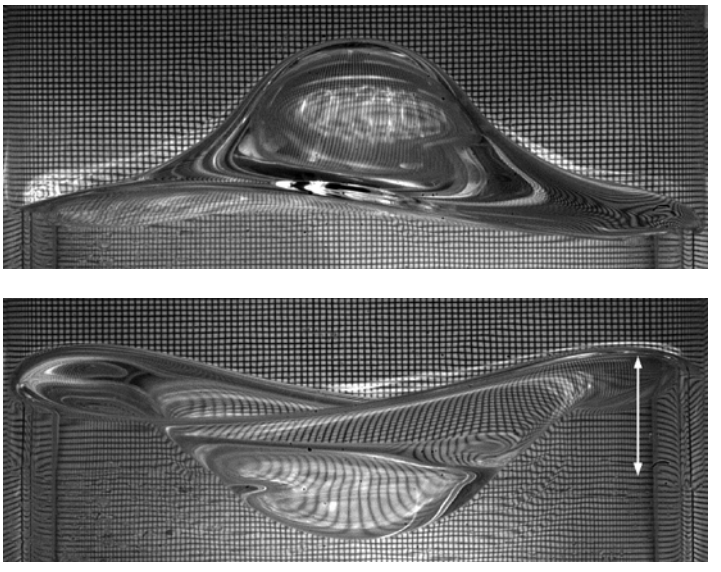


FIGURE 13. Experimental visualization of the (*a*) maximum and (*b*) minimum cycle of the growth of the co-dimension 2 point consisting of a $(2, 1)_{sh}$ mode with a $(0, 1)_{sh}$ mode from the data set in figure 12. See supplementary movie 5.

behaviour as in figure 9. In the case of this instability it should be noted that the film is not azimuthally uniform due to the presence of the $(2, 1)_{sh}$ mode.

Of great interest is the deviation between the thresholds and the predictions in both data sets; the observed 1.5 cSt thresholds clearly provide better agreement with the predictions compared to those of the 10 cSt oil. In fact the sidewall film was much smaller and difficult to notice in the 1.5 cSt oil systems, and therefore, in addition to lower stresses arising from sidewall boundary layers, we concluded that the total sidewall contribution to the overall system dissipation was much smaller when using 1.5 cSt oil. At the end of the section, this will be quantitatively justified by comparison of the predicted interior viscous contribution with the experimental damping rates. Thus, in the interest of ideality, the remainder of the experiments presented used 1.5 cSt oil, which allows us to more carefully pinpoint the interaction between the non-ideality and the instability. Before presenting more threshold data, the nonlinear behaviour of the wave growth will be discussed using figure 12(*a*,*b*) as it is characteristic of all the observed modal behaviour and has a tendency to obscure the linear threshold.

5.3. *Nonlinear growth and saturation*

The nonlinear behaviour changes considerably as one moves from the detuned branch of the $(2, 1)_{sh}$ mode to the tuned branch in figure 12. It has also been reported that the bifurcation is subcritical for frequencies below the natural frequency, i.e. detuned modes, and supercritical for frequencies above the natural frequency, i.e. tuned modes (Miles 1984; Douady 1990). In this work, the experimental observations are consistent with this, given that there exists a 'jump' in the saturated amplitude of the excited mode for the data points at frequencies less than the natural frequency, while at frequencies above the natural frequency the mode saturation is nearly zero at the critical threshold. In fact, for many of the points below the natural frequency, the

https://doi.org/10.1017/jfm.2013.324 Published online by Cambridge University Press

excited mode grows until the interface ruptures for imposed amplitudes slightly above the threshold. Because such a marked change can be observed by such slight changes in the imposed amplitude, detection of the instability is quite easy for the subcritical branch. The instability is more difficult to detect on the supercritical branch, because a slight increase in the imposed amplitudes past the threshold results in only a slight increase in the saturated wave amplitude. This difficulty is compounded for tuned harmonic modes, as it becomes more difficult to differentiate the instability from the meniscus waves, whose emission is also harmonic.

Finally, the temporal dynamics of the growth of detuned modes is very interesting. In the excitation of detuned modes, there were periods of time during which the interface showed no instability well after initialization of the cell motion. Only the meniscus waves persisted during these induction periods, and suddenly the interface would begin to deflect and grow in a rapid manner. These induction times increased with proximity to the critical threshold, sometimes approaching four or five minutes, as noted by Das & Hopfinger (2008).

5.4. *FC70 and 1.5 cSt silicone oil instability thresholds*

Figures 14 and 15 show the sets of threshold data for cells filled with large and small heights of FC70 and 1.5 cSt silicone oil. Frequency bands and threshold amplitudes were found for modes ranging from 2 to ∼8 Hz. Above 8 Hz the wavefield was excited at considerably smaller amplitudes and the system behaved more like a laterally infinite system as the effects of mode discretization began to vanish. In both systems, superharmonic and harmonic modes were observed in addition to the traditional subharmonic response. Co-dimension 2 points, predicted theoretically by the model as the cusps in the stability curve, were found throughout the frequency range by careful actuation of both frequency and amplitude. The experimental thresholds for both layer heights are predicted quite well by the model, especially from the perspective of mode selection. For only a handful of points is the observed mode different from the theoretical prediction. However, there are certainly some noticeable trends of the data not matching the predictions, and for this reason, the results of each cylinder will be discussed separately.

The experimental data are grouped together according to mode. The system presented in figure 14 is the large height system with an FC70 layer of 3.1 cm and a 1.5 cSt silicone oil layer of 3.3 cm. The modes observed in this system, in increasing frequency, are $(1,1)_h$, $(1,2)_{su}$, $(2,1)_h$, $(0,1)_h$, $(3,1)_h$, $(1,2)_h$, $(1,1)_{sh}$, $(2,1)_{sh}$, and $(0,1)_{sh}$, for which the Bond numbers ranged from ∼50 to 400. The observed modes, denoted by the enclosing boxes in the figure, match the predicted mode except when noted. The threshold amplitudes show good agreement, save for the points near the tongue minima for the subharmonic and superharmonic modes, due to residual wall dissipation. On the other hand, for the $(0,1)_h$ and $(1,2)_h$ tongues, it can be clearly seen that the thresholds of the experiment lie below the predicted thresholds. This is a noteworthy result, and the best explanation seems to be the interaction of the harmonic, axisymmetric meniscus waves with the instability, lending itself to thresholds below the prediction.

A similar set of modes were observed for experiments with reduced layer heights, where an FC70 layer of $h_1 = 2.1$ cm and a 1.5 cSt layer of $h_2 = 2.0$ cm were used (see figure 15). The effect of layer heights from the inviscid theory for two liquids was shown by Kumar & Tuckerman (1994) where height dependence in the dispersion

https://doi.org/10.1017/jfm.2013.324 Published online by Cambridge University Press

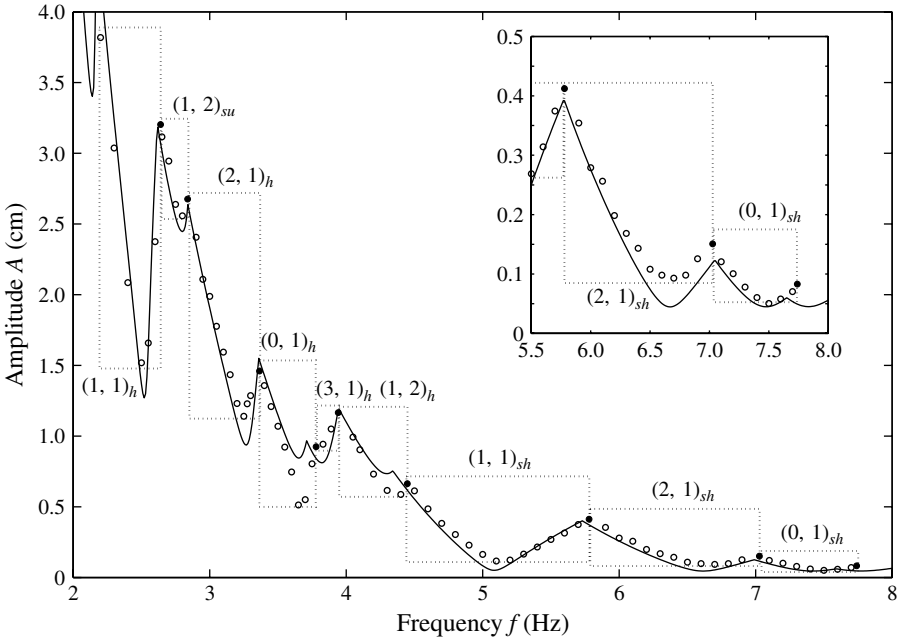


FIGURE 14. Experimental and predicted thresholds of instability for a bilayer of FC70 ($h_1 = 3.1$ cm, $\rho_1 = 1888$ kg m^{-3}) and 1.5 cSt silicone oil ($h_2 = 3.3$ cm, $\rho_2 = 846$ kg m^{-3}). Data points enclosed by a box indicate the excited mode. Black dots represent co-dimension 2 points.

relation arises via the expression

$$\frac{\rho_1 + \rho_2}{\rho_1 \coth kh_1 + \rho_2 \coth kh_2},$$

which shows saturation toward unity when kh_1 and kh_2 are greater than $\sim$3. In this system, the expression leads to values of 0.89 for the (1, 1) modes, 0.98 for the (2, 1) modes, and 0.99 for the (0, 1) modes, indicating only a moderate effect of height. Still, the resulting shift of the harmonic and subharmonic (1, 1) modes are observed as predicted by the viscous theory. However, it should be noted that the $(1, 2)_h$ mode observed between 4 and 4.4 Hz just above threshold is not the predicted mode. The predicted threshold for the $(1, 2)_h$ mode is shown in figure 15 and is predicted to be higher than the $(1, 1)_{sh}$ mode. The early presence of the $(1, 2)_h$ mode observed in the small and large height systems gives further reason to believe in the existence of an interaction with the meniscus waves. The ordering of the modes in figure 15 is largely the same as seen for the large height system, save for the region from 3.8 to 4 Hz, where instead of only $(3, 1)_h$ modes a $(4, 1)_h$ mode was also observed. The predicted $(3, 1)_h$ mode was damped considerably. Also absent from the experimental system are the $(4, 1)_h$ modes, predicted around 2.6 Hz. The trend here appears to be that wall damping increases substantially with the number of azimuthal nodes and therefore also a decrease in the Bond number. It is clearly noticeable in the low height system that the $(0, 1)_h$ thresholds are again much lower than predicted, for the same reason as given earlier for the large height system.

https://doi.org/10.1017/jfm.2013.324 Published online by Cambridge University Press

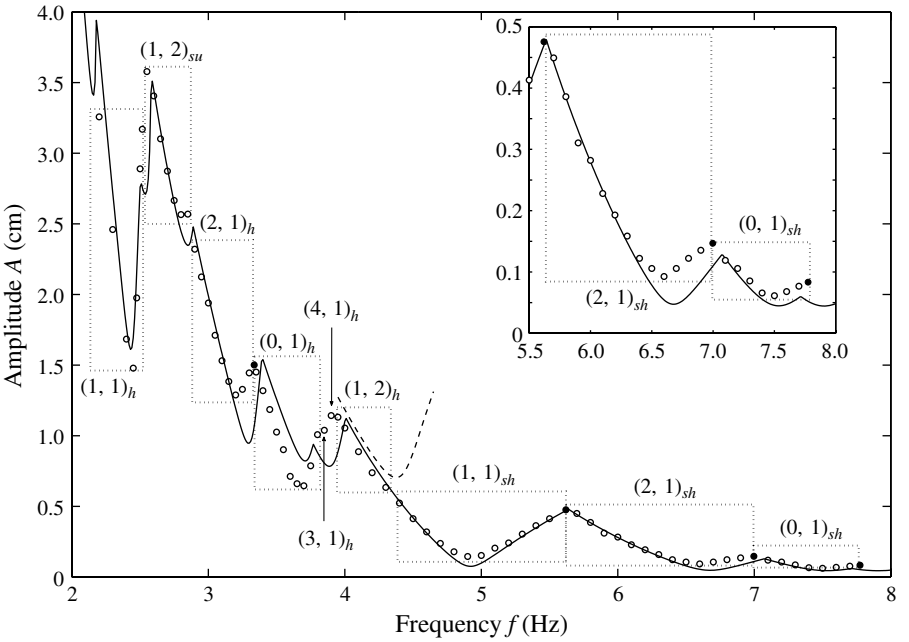


FIGURE 15. Experimental and predicted thresholds of instability for a bilayer of FC70 ($h_1 = 2.1$ cm, $\rho_1 = 1916$ kg m^{-3}) and 1.5 cSt silicone oil ($h_2 = 2.0$ cm, $\rho_2 = 846$ kg m^{-3}). The dashed line represents the predicted $(1, 2)_{sh}$ threshold.

5.5. *Saturated interface amplitudes*

Figure 16(*a*,*b*) presents the saturated wave amplitude with respect to the imposed vibrational amplitude in the large height system (see figure 14) for two different frequencies, roughly corresponding to the natural frequencies of the $(1, 1)_h$ and $(0, 1)_h$ modes. Here the wave amplitude has been taken as half the difference between the maximum and minimum interfacial heights. The general shapes of the response of figure 16(*a*,*b*) resemble those of Henderson & Miles (1990) and Das & Hopfinger (2008), but what is intended to be shown is smoothing of the response near the critical threshold as opposed to a sharp bifurcation. This smoothing of the response near the threshold represents an imperfect bifurcation. This was first observed and described as a 'tailing' by Virnig, Berman & Sethna (1988), who reported similar behaviour for the wave response of $(1, 1)_{sh}$ modes in a rectangular cell using water. Addition of surfactant minimized the tailing in their experiments. In contrast to their observation of this behaviour for a subharmonic mode, the tailing in the current work seems be characteristic of the interaction with the meniscus waves, as was additionally noticed for the $(2, 1)_h$ mode, but was nearly absent for the $(1, 1)_{sh}$, $(2, 1)_{sh}$ and $(0, 1)_{sh}$ modes.

5.6. *System damping study*

To quantify the damping in the system, the (0, 1) mode was both harmonically and subharmonically excited in the FC70 and 10 cSt silicone oil system and also in the large and small height FC70 and 1.5 cSt silicone oil systems. A total of eight measurements of the decay of an excited $(0, 1)_h$ mode for the 10 cSt system were taken at excitation frequencies of 3.3 and 3.4 Hz with imposed amplitudes of 15 and 16 mm. Analysis of the time series of the wave amplitudes at the centre of

https://doi.org/10.1017/jfm.2013.324 Published online by Cambridge University Press

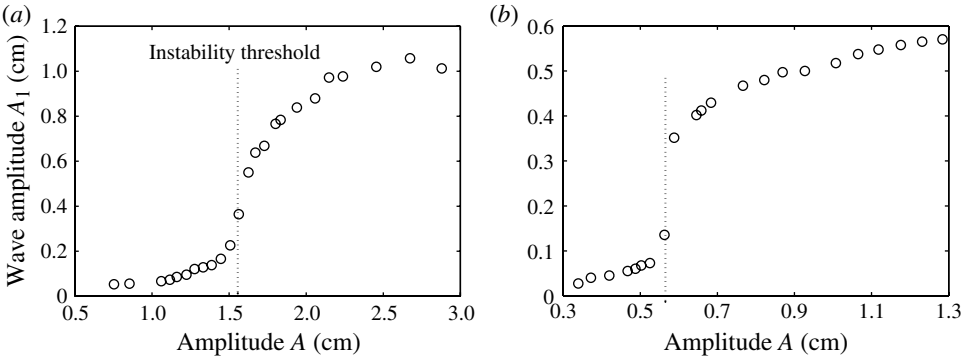


FIGURE 16. Wave amplitude responses for the large height system (see figure 14) for imposed frequencies of (*a*) 2.52 Hz and (*b*) 3.68 Hz.

the cell yielded an average damping rate of 1.15 s^{-1}. Measurements for the $(0, 1)_{sh}$ mode were taken at frequencies of 7 and 7.1 Hz with imposed amplitudes of 2.2 and 2.3 mm, yielding an average rate of 1.12 s^{-1}. Calculation of the linear viscous contribution from the interior with (3.2) predicts a rate of 0.51 s^{-1} for both the harmonic and subharmonic modes, suggesting that the remainder might be attributed to wall effects. Damping measurements for similar forcing parameters in the 1.5 cSt silicone oil systems yielded harmonic and subharmonic damping rates of 0.65 and 0.67 s^{-1} in the large height system and 0.58 and 0.57 s^{-1} in the small height systems. Here the interior contributions from (3.2) are 0.397 and 0.395 s^{-1} for the small and large height systems, respectively. Comparison of the interior viscous damping to the overall measured damping reveals the sidewall effects of roughly 0.6 s^{-1} in the 10 cSt system and 0.18–0.25 s^{-1} in the 1.5 cSt systems. We can therefore conjecture that an upper fluid viscosity has a great effect on the dissipation owing to the film formation, as the thickness of this film was noticeably smaller for the experiments with 1.5 cSt silicone oil as opposed to the 10 cSt oil. Henderson & Miles (1990) and Das & Hopfinger (2008) report measured $(0, 1)_{sh}$ decay rates of ∼0.38 and 0.45 s^{-1}, whereas the interior contributions are 0.022 and 0.0049 s^{-1}.

6. Discussion and conclusions

We have designed and presented the results of a discrete-mode Faraday system whose dissipation arises primarily from the interior bulk domains. Previously, low-viscosity fluids resulted in systems whose damping was controlled by sidewall and interfacial dissipative behaviour, resulting in linear thresholds that exhibit various forms of mismatch with a viscous fluid model when the walls are taken to be stress-free: see figure 6. The results of the current work, however, show remarkable agreement with this theory, especially with regard to mode selection and the positioning of the co-dimension 2 points. This stands in contrast to a statement of Henderson & Miles (1990), who did experiments in both circular and rectangular cylinders, and who concluded that the linear stability theory may not be valid in the region where two modes are unstable. We simply find this not to be true, evident by the accuracy of the viscous linear theory's prediction of the co-dimension 2 points in figures 14 and 15. Their conclusion was drawn with regard to the excitation of neighbouring $(4, 0)_{sh}$ and $(3, 1)_{sh}$ modes in a rectangular cylinder. In the region of the

https://doi.org/10.1017/jfm.2013.324 Published online by Cambridge University Press

stability diagram where the two modes intersect, Henderson & Miles (1990) observed only the emergence of the $(4, 0)_{sh}$. They attributed this to the lower measured damping rate of the mode when compared to the rate of the $(3, 1)_{sh}$ mode. This result was, however, obtained from experiments in a rectangular cell and therefore it is difficult to say whether or not it coincides with our claim that increasing azimuthal nodes causes the suppression of a mode.

The threshold amplitudes at which certain modes appear in the current work do, however, show deviation from the predictions, and the deviation can separately be attributed to the sidewall damping and meniscus waves. Past reports have struggled to model and provide description of the sidewall behaviour, and we believe that the film behaviour observed in this work is unique in its simplicity. Ito & Kukita (2008) attempted to model the nonlinear relationship between the contact angle and the contact line speed in such a film, given the effects of hysteresis and non-uniform wetting of the two phases, and applied it to the excitation of the fundamental axisymmetric mode. Creation of such a film appears to be dependent upon the preferential sidewall wetting of one of the two phases and minimization of the associated stresses can be achieved if this phase is of low viscosity. Furthermore, it is our belief that a low interfacial tension encourages the film forming process, as the energy requirement to bend the surface from its actual contact position and then stretch it vertically over the silicone oil film, is high: see figures 10 and 11.

The other aspect of the non-ideality is the meniscus waves, whose effect on the linear threshold has not been previously observed and is most simply thought of as forced oscillations, which interact with the parametric wave. Figures 14 and 15 clearly show how the threshold can be altered due to the interaction of the meniscus waves with the instability for the $(0, 1)_h$ and $(1, 2)_h$ modes. This alteration is mathematically interesting, as the forced oscillations owing to the meniscus could possibly be modelled using a periodic inhomogeneity in (2.15). This approach was taken by Tipton (2003), who numerically showed that the neutral curves were adjusted when the linearly damped Mathieu equation was forced with such an inhomogeneity. This study, however, was done for destabilization of the base harmonic solution (i.e. meniscus waves) to a subharmonic solution, whereas our experiments showed measurable interaction for only harmonic modes. A periodic inhomogeneity was also incorporated by Ito *et al.* (1999) with their model for their Faraday experiment. Recall that their experiment used a piston to oscillate a column of water and kerosene up and down in a pipe, generating both a sidewall film and sidewall fluid shearing in their base state, thereby preventing a classical Faraday description. However, the system remains qualitatively similar and the periodicity of these perturbations is identical to that of the meniscus waves. Their final equation is a linearly damped Mathieu equation with the addition of such a periodic inhomogeneity, but analysis was not performed to show how the harmonic modes interact with the inhomogeneity.

A concern in applying such a model to these experiments includes the vanishing of this interaction due to the mismatch of the spatial forms of the axisymmetric meniscus waves and the cell modes of higher azimuthal index. This is seen as one compares the experimental thresholds for the $(0, 1)_h$, $(1, 2)_h$, $(1, 1)_h$, and the $(2, 1)_h$ modes in figures 14 and 15. The interaction remains present in the $(1, 2)_{sh}$ mode but has apparently vanished with the $(2, 1)_h$ mode. We argue that the interaction is still present for the $(1, 1)_h$ mode, considering that the thresholds appear to hit the tongue minimum predicted by viscous linear stability theory, in contrast to the analogous $(1, 1)_{sh}$ mode, for which this does not happen (due to wall dissipation). Thus it appears that the diminishing magnitude of the interaction can be attributed to the increasing number

https://doi.org/10.1017/jfm.2013.324 Published online by Cambridge University Press

of azimuthal nodes. This description is easiest for the $(0, 1)_h$ mode due to agreement of the spatial symmetry with the meniscus waves. Another important consideration is the imperfect bifurcation presented in figures 16(*a*) and 16(*b*), which emphasize the varying amplitudes of the meniscus waves near the thresholds.

Further discussion of the previous work can now be made and much of the disagreement between the experiments of these earlier works and the theory can be explained. The absence of the $(4, 1)_{sh}$ mode in the experiments of Benjamin & Ursell (1954) is probably due to the large wall dissipation relative to the observed $(1, 2)_{sh}$ mode, and the same reason applies to the absence of the $(3, 1)_{sh}$ mode in the experiments of Tipton & Mullin (2004). We find the experiments of Dodge *et al.* (1965) to be interesting due to the large diameter system used and the seemingly minimal amount of tongue damping observed in their $(1, 1)_{sh}$ thresholds, especially when compared to $(1, 1)_{sh}$ thresholds of this work. The failure of the Kumar & Tuckerman model to predict the thresholds of Henderson & Miles (1990), Tipton & Mullin (2004) and Das & Hopfinger (2008) further highlights both the complexity of damping in single-mode Faraday experiments and also therefore the advantages of designing a system whose damping is linear. We believe the use of a viscous system and the comparison with a rigorous model that incorporates viscosity has been instrumental in pinpointing the meniscus wave interaction.

A final note ought to be given regarding the nonlinear behaviour of the system, as its presence pervaded and sometimes obscured the precise measurement of the linear thresholds. Mode amplitudes in single-mode systems have been measured by Dodge *et al.* (1965), Tipton & Mullin (2004) and Das & Hopfinger (2008). The most common observations are the transitions from a subcritical to supercritical bifurcation as the parametric frequency increases past the tongue minima. Both Virnig *et al.* (1988) and Henderson & Miles (1990) compared the measured wave amplitudes to weakly nonlinear phenomenological theories which include dissipation. The most complete weakly nonlinear theory is that of Skeldon & Guidoboni (2007), who rigorously extended the Kumar & Tuckerman model into the nonlinear regime with interest in pattern formation. Adapting their work to a cylindrical discretized system for the prediction of mode amplitudes and branching behaviour could offer further insight into this unique experimental system. The last and perhaps least understood phenomenon, indescribable by a weakly nonlinear theory, are the induction times observed on the subcritical branches of the instability. Das & Hopfinger (2008) present data for which the temporal growth of a mode can be modelled by an exponential behaviour with a time lag, this time lag corresponding to the induction period where no cell activity is observed. In light of the present discussion of the sidewall non-ideality, one possible explanation may be that the cell dynamics induced by the meniscus wave perturbations, which, once shaking is initialized, are required to reach a certain state before a jump to Faraday resonance can occur.

In summary, the Faraday linear stability theory adapted for a confined cylindrical geometry has been shown to be excellent for predicting both the experimental threshold and mode of instability for a wide range of subharmonic, harmonic, and superharmonic responses. This agreement was achieved using a two-liquid immiscible system characterized by its generation of a sidewall film, and the minimization of the viscosity of the fluid forming this film improved the agreement. Persistent deviation between the observed and predicted thresholds appears only for the modes harmonic with the parametric forcing, owing to an interaction with the harmonic capillary waves emitted from the sidewall meniscus.

https://doi.org/10.1017/jfm.2013.324 Published online by Cambridge University Press

Acknowledgements

W.B. and R.N. acknowledge support from NASA NNX11AC16G, NSF 0968313, and a Chateaubriand Fellowship. F.Z. acknowledges support from CNRS-CNES and a Marie Curie International Research Staff Exchange Scheme Fellowship within the 7th European Community Framework Programme. We additionally acknowledge the anonymous referees, whose helpful responses to the initial fast track submission dramatically increased both the focus and the detail of the investigation.

Supplementary movies

Supplementary movies are available at http://dx.doi.org/10.1017/jfm.2013.324.

REFERENCES

ABRAMOWITZ, M. & STEGUN, I. A. 1964 *Handbook of Mathematical Functions*, 10th edn. Dover.

BECHHOEFER, J., EGO, V., MANNEVILLE, S. & JOHNSON, B. 1995 An experimental study of the onset of parametrically pumped surface waves in viscous fluids. *J. Fluid Mech.* **288**, 325–350.

BENJAMIN, T. B. & URSELL, F. 1954 The stability of a plane free surface of a liquid in vertical periodic motion. *Proc. R. Soc. Lond.* A **225**, 505–515.

CASE, K. M. & PARKINSON, W. C. 1957 Damping of surface waves in an incompressible fluid. *J. Fluid Mech.* **2**, 172–184.

CHRISTIANSEN, B., ALSTRØM, P. & LEVINSEN, M. T. 1994 Dissipation and ordering in capillary waves at high aspect ratios. *J. Fluid Mech.* **291**, 323–341.

CILIBERTO, S. & GOLLUB, J. P. 1985 Chaotic mode competition in parametrically forced surface waves. *J. Fluid Mech.* **158**, 381–398.

DAS, S. P. & HOPFINGER, E. J. 2008 Parametrically forced gravity waves in a circular cylinder and finite-time singularity. *J. Fluid Mech.* **599**, 205–228.

DODGE, F. T., KANA, D. D. & ABRAMSON, H. N. 1965 Liquid surface oscillations in longitudinally excited rigid cylindrical containers. *AIAA J.* **3**, 685–695.

DOUADY, S. 1990 Experimental study of the Faraday instability. *J. Fluid Mech.* **221**, 383–409.

FAUVE, S., KUMAR, K., LAROCHE, C., BEYSENS, D. & GARRABOS, Y. 1992 Parametric instability of a liquid–vapor interface close to the critical point. *Phys. Rev. Lett.* **68** (21), 3160–3163.

FRIEND, J. & YEO, L. Y. 2011 Microscale acoustofluidics: microfluidics driven via acoustics and ultrasonics. *Rev. Mod. Phys.* **83**, 647–704.

HENDERSON, D. & MILES, J. 1990 Single-mode Faraday waves in small cylinders. *J. Fluid Mech.* **213**, 95–109.

ITO, T. & KUKITA, Y. 2008 Interface behavior between two fluids vertically oscillated in a circular cylinder under nonlinear contact line condition. *J. Fluid Sci. Technol.* **3**, 690–711.

ITO, T., TSUJI, Y. & KUKITA, Y. 1999 Interface waves excited by vertical vibration of stratified fluids in a circular cylinder. *J. Nucl. Sci. Technol.* **36**, 508–521.

KEULEGAN, G. H. 1958 Energy dissipation in standing waves in rectangular basins. *J. Fluid Mech.* **6**, 33–50.

KITYK, A. V., EMBS, J., MEKHONOSHIN, V. V. & WAGNER, C. 2005 Spatiotemporal characterization of interfacial Faraday waves by means of a light absorption technique. *Phys. Rev.* E **72**, 036209.

KUMAR, K. 1996 Linear theory of Faraday instability in viscous fluids. *Proc. R. Soc. Lond.* A **452**, 1113–1126.

KUMAR, K. & TUCKERMAN, L. 1994 Parametric instability of the interface between two fluids. *J. Fluid Mech.* **279**, 49–67.

LANDAU, L. D. & LIFSHITZ, L. M. 1987 *Fluid Mechanics*, vol. 6. Course of Theoretical Physics, Butterworth-Heinemann.

MILES, J. W. 1967 Surface-wave damping in closed basins. *Proc. R. Soc. Lond.* A **297**, 459–475.

MILES, J. W. 1984 Nonlinear Faraday resonance. *J. Fluid Mech.* **146**, 285–302.

https://doi.org/10.1017/jfm.2013.324 Published online by Cambridge University Press

MILNER, S. T. 1991 Square patterns and secondary instabilities in driven capillary waves. *J. Fluid Mech.* **225**, 81–100.

MÜLLER, H. W., WITTMER, H., WAGNER, C., ALBERS, J. & KNORR, K. 1997 Analytic stability theory for Faraday waves and the observation of the harmonic surface response. *Phys. Rev. Lett.* **78** (12), 2357–2360.

NAYFEH, A. H. & MOOK, D. T. 1979 *Nonlinear Oscillations*. Wiley.

SKELDON, A. C. & GUIDOBONI, G. 2007 Pattern selection for Faraday waves in an incompressible fluid. *SIAM J. Appl. Maths.* **67** (4), 1064–1100.

SOMEYA, S. & MUNAKATA, T. 2005 Measurement of the interface tension of immiscible liquids interface. *J. Cryst. Growth* **275**, 343–348.

TIPTON, C. 2003 Interfacial Faraday waves in a small cylindrical cell. PhD thesis, University of Manchester.

TIPTON, C. R. & MULLIN, T. 2004 An experimental study of Faraday waves formed on the interface between two immiscible liquids. *Phys. Fluids* **16**, 2336–2341.

VIRNIG, J. C., BERMAN, A. S. & SETHNA, P. R. 1988 On three-dimensional nonlinear subharmonic resonant surface waves in a fluid. Part 2. Experiment. *Trans. ASME E: J. Appl. Mech.* **55**, 220–224.

WAGNER, C., MÜLLER, H.-W. & KNORR, K. 2003 Pattern formation at the bicritical point of the Faraday instability. *Phys. Rev.* E **68**, 066204.

ZOUESHTIAGH, F., AMIROUDINE, S. & NARAYANAN, R. 2009 Experimental and numerical study of miscible Faraday instability. *J. Fluid Mech.* **628**, 43–55.

https://doi.org/10.1017/jfm.2013.324 Published online by Cambridge University Press